Proceedings of the 11th World Congress on Mechanical, Chemical, and Material Engineering (MCM'25)

Paris, France - August, 2025 Paper No. ICCPE 141 DOI: 10.11159/iccpe25.141

# Comparison of UiO-66 Nanoparticles Synthesized via Micro-fluidic vs. Macro-Stationary Routes for Aqueous Phosphate Removal

# Buket Ustun<sup>1,2</sup>, Selis Onel<sup>1\*</sup>

<sup>1</sup>Hacettepe University, Department of Chemical Engineering
Beytepe, Ankara, Turkiye

<u>ustun.buket@metu.edu.tr</u>, <u>selis@hacettepe.edu.tr</u>

<sup>2</sup>Middle East Technical University, Department of Chemical Engineering
Ankara, Turkiye

**Abstract** – Phosphate contamination in wastewater is a critical environmental concern, driving eutrophication. This study investigates the synthesis of zirconium-based UiO-66 metal organic framework (MOF) nanoparticles via conventional macro-stationary batch and droplet-based micro-fluidic systems for phosphate removal from aqueous solutions. Characterization using XRD and SEM revealed that micro-fluidically synthesized UiO-66 nanoparticles exhibited smaller crystallites and higher crystallinity compared to those from the macro-stationary method. Adsorption kinetics followed a pseudo-second-order model and the Freundlich isotherm provided a better fit to the equilibrium data. Thermodynamic analysis indicated a spontaneous physisorption process. Comparative adsorption studies showed that UiO-66 nanoparticles synthesized via the micro-fluidic route demonstrated slightly enhanced phosphate removal efficiency. This work highlights the potential of micro-fluidic synthesis for producing MOF nanoparticles with improved properties for environmental applications.

Keywords: Phosphate removal, UiO-66, Metal organic framework (MOF), Two-phase micro-fluidics

## 1. Introduction

Phosphate contamination in wastewater poses a significant environmental threat to aquatic ecosystems and compromises access to clean water resources. Eutrophication in lakes remains as a persistent problem for the environment and is caused by over-enrichment with phosphorus [1]. Large amounts of nitrogen and phosphorus are released into water due to obligatory anaerobic treatment of domestic and agro-industrial wastewater. Many methods have been developed throughout the years to treat the excess amounts of phosphate in water bodies, such as precipitation by metal salts, cultivation of microorganisms in wastewater and wetland construction [2]. More recently, adsorption-based technologies have emerged as promising alternatives due to their potential for high efficiency and material versatility. Powdered natural pumice rock has been used by Onar et al. [3] in 1995 and has shown an adsorption capacity of  $0.95 \pm 0.07$  mg/g. Mei et al. [4] investigated the performance of sand, iron powder, and aluminum powder, achieving maximum adsorption capacities of 2.9163, 1.3328, 2.5849 mg/g, respectively. He et al. [5] studied the inherent porosity of zeolites for phosphate removal and showed a significantly enhanced adsorption capacity of 17.2 mg/g for lanthanum-incorporated porous zeolite. Metal organic framework (MOF) structures, created from inorganic ions with organic connectors, have emerged as a class of materials with adaptable structure, flexible functionality, variable composition, and high porosity [6]. In the synthesis of particles with MOF structures, rational combinations of metal ions and organic ligands produces materials with various pore sizes and connectivity, theoretically allowing for an almost infinite number of possible configurations [7]. MOFs have demonstrated significant potential for real-world implementation areas, such as gas storage, molecular sensing, separation, and enrichment [8]. Their low densities (0.2–1 g/cm<sup>3</sup>), large surface areas (500–6500 m<sup>2</sup>/g), pore sizes of wide ranges, and improved thermal and mechanical stabilities make them promising materials specifically for separation processes [7]. These properties have also been proven to be useful for adsorption mechanics. The conventional method of producing MOFs is solvothermal synthesis, typically carried out in batch reactors at elevated temperatures. However, this macro-scale approach can exhibit limitations, such as batch-to-batch variability and suboptimal control over synthesis parameters. In this context, micro-fluidic synthesis offers a compelling alternative.

Micro-fluidic platforms for droplet generation include capillary-based devices and micro-structured chips with diverse geometric designs, which can provide a homogeneous synthesis environment and optimal control over parameters [9]. These

microsystems can be broadly categorized based on their mechanism of droplet formation, which involves the controlled emulsification or segmentation of reactant solutions. In planar t-junction or x-junction flow focusing two-phase microfluidic devices, the continuous and dispersed fluids move through microchannels. Conversely, capillary-based droplet devices typically employ a configuration, where the continuous phase flows through a larger channel, while the dispersed phase is introduced via a fine capillary tip, with the common objective of inducing liquid thread breakup into discrete droplets [9, 10]. X-junction micro-fluidic devices have gained prominence for their capacity to accommodate higher flow-rate ratios and a wider range of operational conditions compared to t-junction systems [11]. Consequently, microfluidic systems present themselves as promising platforms for the controlled synthesis of MOFs, offering enhanced control over reaction kinetics, particle size, and morphology.

In this study, nanoparticles exhibiting the zirconium (Zr) based UiO-66 MOF crystalline structure were synthesized using two distinct methodologies: a conventional macro-scale batch process and a two-phase droplet-based micro-fluidic system. Zr-UiO-66 nanoparticles produced via two different approaches were identified and analyzed via x-ray diffraction (XRD) and scanning electron microscope (SEM) analyses. The phosphate adsorption capacity of the resultant Zr-UiO-66 nanoparticles from both synthesis routes was subsequently evaluated.

#### 2. Materials and Method

The precursor solution was prepared using zirconium (IV) chloride (ZrCl<sub>4</sub>) as the metal salt, terephthalic acid ( $H_2BDC$ ,  $C_8H_6O_4$ ) as the organic ligand, and n,n-dimethylformamide (DMF, (CH<sub>3</sub>)<sub>2</sub>NC(O)H, 99.8%) as the solvent. Hydrochloric acid (HCl, 37%) and deionized water functioned as modulators during synthesis. All chemicals used in the experiments were purchased commercially in analytical grades from Sigma Aldrich (St. Louis, Missouri, USA) unless stated otherwise. Following synthesis, the particles were purified by sequential washing with DMF and acetone. All reagents in the precursor solution were measured precisely using an analytical balance for solids and calibrated micropipettes for liquids. The phosphate adsorption capacity of UiO-66 nanoparticles from both synthesis routes was assessed using the phosphate solutions as the adsorbate model. Phosphate solutions simulating polluted water were prepared using potassium dihydrogen phosphate (KH<sub>2</sub>PO<sub>4</sub>, ACS Reagent grade). Residual phosphate concentrations were determined spectrophotometrically using the molybdenum blue method, prepared with concentrated sulfuric acid (H<sub>2</sub>SO<sub>4</sub>, 99.8%), ascorbic acid (C<sub>6</sub>H<sub>8</sub>O<sub>6</sub>), and ammonium molybdate tetrahydrate ((NH<sub>4</sub>)<sub>6</sub>Mo<sub>7</sub>O<sub>24</sub>.4H<sub>2</sub>O).

## 2.1. Macro-Stationary Synthesis

The macro-stationary batch synthesis procedure targeted a final precursor solution composition with a molar ratio formulation of ZrCl<sub>4</sub>:H<sub>2</sub>BDC:DMF:HCl:H<sub>2</sub>O equivalent to 1:1:80:2:20. For the preparation of 20 mL of the final precursor solution, 10 mL of DMF was added to two separate test tubes. 0.7525 g of ZrCl<sub>4</sub> was added to the first test tube and 0.5364 g of H<sub>2</sub>BDC was added to the other one. Both test tubes were subjected to mixing in an ultrasonic mixer for a minimum of 30 minutes until complete dissolution was visually confirmed by the formation of homogeneous, transparent solutions. The contents of the two test tubes were combined and allowed to equilibrate for 10 minutes. 200  $\mu$ L of HCl and 1163  $\mu$ L of deionized water were sequentially added followed by an additional 10 minutes of ultrasonication to ensure homogeneity. Following precursor preparation, the solution was transferred to a 20 mL glass vial, sealed, and placed in an oven maintained at 100 °C for a synthesis period of 30 minutes. Post-synthesis, a white, gel-like precipitate was observed suspended in the solvent. To isolate the solid product, the mixture was centrifuged at 5000 rpm for 10 minutes. A washing procedure was implemented involving the resuspension of the solid product followed by centrifugation at 5000 rpm for 10 minutes for each wash cycle. This procedure entailed three wash cycles using DMF followed by two wash cycles using acetone. After the final wash and decantation of the supernatant, the purified product was dried overnight in an oven at 80 °C.

#### 2.2. Micro-Fluidic Synthesis

For synthesis using the micro-fluidic system, the precursor solution was prepared using the identical formulation and molar ratios (ZrCl<sub>4</sub>:H<sub>2</sub>BDC:DMF:HCl:H<sub>2</sub>O = 1:1:80:2:20) as employed in the macro-scale batch method. The total preparation volume was scaled down to 2 mL. Precursor solution, serving as the dispersed phase, was loaded into a 1 mL syringe. Continuous phase consisted of silicone oil, prepared by pre-saturating with 20% v/v DMF, followed by the addition

of 0.1% v/v Span80 and 0.1% v/v AOT as surfactants. The continuous phase was divided and loaded into two separate 1 mL syringes. Syringes containing the dispersed and continuous phases were connected via polytetrafluoroethylene (PTFE) microtubing (ID 0.3 mm, OD 0.76 mm, Masterflex Transfer Tubing, Avantor, Inc, USA) to a flow-focusing micro-fluidic device featuring an x-junction geometry. The outlet of the micro-fluidic device was extended with a 1.5-meter length of PTFE microtubing (ID 0.6 mm, OD 1.3 mm, Deutsch & Neumann GmbH, Germany), routed through an oven maintained at 100 °C, and terminated in a product collection vessel. The length of the tubing was arranged to achieve a 30 minute-residence time for the precursor solution within the heated zone based on operational flow rates. Fluid delivery was controlled using Nemesys BASE120 syringe pumps (CETONI GmbH, Germany). Initially, all syringe pumps were set to a flow rate of 3.4  $\mu$ L/min. The flow rate for the dispersed phase (precursor solution) was gradually decreased by 1  $\mu$ L/min at 10-minute intervals until a stable flow rate of 0.5  $\mu$ L/min was attained. These operational flow rates were determined by prior optimization studies. Following the arrangement of flow rates, the synthesized product was directed to a waste collection tube for 30 minutes to ensure the system reached steady state. Once stable product formation was observed, the outlet tubing was redirected to the designated product collection tube. The collected solid product was subjected to washing and drying protocols identical to those used in the macro-stationary batch synthesis.

#### 2.3. Phosphate Adsorption

To examine the phosphate adsorption capabilities of the synthesized UiO-66, kinetic adsorption experiments were conducted. Aqueous stock solutions of phosphate (PO<sub>4</sub><sup>3-</sup>) were prepared at initial concentrations of 25, 50, 75, and 100 mg/L to simulate potential wastewater compositions. For each concentration, experiments were initiated by adding 0.03 g of the macro-stationary synthesized UiO-66 particles to 30 mL of the phosphate solution resulting in an adsorbent dosage of 1 g/L. The suspensions were maintained under continuous agitation using magnetic stirrer at 500 rpm to ensure homogeneity. 2 mL aliquots were withdrawn from the suspension at 1, 5, 10, 15, 20, 30, 45, 60, 90, and 120 minutes without interrupting the stirring. The adsorbent UiO-66 particles within each aliquot were separated from the liquid phase via centrifugation. The supernatant, containing the residual phosphate, was collected for quantitative analysis. Owing to the limited UiO-66 yield from the micro-fluidic synthesis route, the adsorption evaluation for this case was modified. Experiments were conducted using 0.01 g of the micro-fluidic-synthesized UiO-66 added to a 10 mL solution of 75 mg/L phosphate concentration, maintaining the adsorbent dosage of 1 g/L. Following the same agitation and sampling protocols, consequent to the limited material, aliquot withdrawal was restricted to earlier time points of 1, 5, 10, 15, 20 minutes. Sample processing via centrifugation and supernatant collection followed the same protocol. Residual phosphorus concentrations in all collected supernatant samples were quantified using ultraviolet-visible (UV-Vis) spectroscopy (GENESYS 180, Thermo Scientific, USA).

### 2.4. Phosphate Quantification

Phosphate quantification methods that have been used previously identified the molybdenum blue spectrophotometric method as a widely utilized and appropriate approach for this study. Molybdenum blue colorimetric reagent was freshly prepared daily according to the recipe adapted from Chen et al. [12]. The reagent was prepared by mixing 1 volume of 6 N H<sub>2</sub>SO<sub>4</sub> solution, 2 volumes of distilled water, 1 volume of 2.5% w/v ammonium molybdate ((NH<sub>4</sub>)6Mo<sub>7</sub>O<sub>24</sub>·4H<sub>2</sub>O, BDH Laboratory Reagents, England) solution, and 1 volume of 10% w/v ascorbic acid (C<sub>6</sub>H<sub>8</sub>O<sub>6</sub>) solution. Initial analysis, by adding the molybdenum blue reagent to the phosphate solutions at a 1:1 ratio, initiated the colorimetric reaction, which resulted with a blue hue within a few minutes, indicative of the phospho-molybdenum complex. This developed color exceeded the linear dynamic detection limits of the UV-Vis spectrophotometer. Therefore, prior to analysis, the supernatant samples collected from adsorption experiments were first diluted with distilled water to a volume ratio of 1:10. Colorimetric reaction was initiated by mixing the diluted sample with freshly prepared molybdenum blue reagent in 1:1 volumetric ratio. Due to the high intensity of the developed blue color, an additional dilution was performed to the ratio of 1:4, resulting in a total dilution of 1:40 by volume. Final absorbance was measured via UV-Vis spectrophotometry at a wavelength of 820 nm to determine the residual phosphate concentration via a calibration curve prepared using standards of known phosphate concentration.

#### 3. Results and Discussion

The findings demonstrate the crystalline structures and phosphate adsorption kinetics of Zr-UiO-66 synthesized via two distinct approaches. Characterization was performed using XRD and SEM analyses.

## 3.1 Characterization of Zr-UiO-66 Nanoparticles

XRD patterns of UiO-66 synthesized through both conventional macro-stationary and micro-fluidic methods were analyzed and validated against a simulated pattern shown in Figure 1. Both synthesis methods successfully produced UiO-66, as evidenced by characteristic diffraction peaks, particularly the distinct doublet around 7.4° and 8.5° 20. The synthesis method significantly influenced the material's properties. As detailed in Table 1, micro-fluidic (MF) route yielded UiO-66 with smaller crystallite sizes and higher crystallinity compared to the macro-stationary route. This is consistent with the broader XRD peaks observed for the UiO-66 MF sample in Figure 1, indicating a smaller crystallite domain. Particle morphology was further investigated using SEM presented with a 500 nm scale bar in Figure 2. Average particle sizes, quantified from SEM micrographs using the ImageJ image analysis tool tabulated in Table 1, corroborated the XRD findings. The micro-fluidic synthesis consistently yielded particles with reduced average dimensions compared to the traditional macro-stationary process. This is attributed to the inherent advantages of micro-fluidic reactors, which offer significantly higher surface-area-to-volume ratios, leading to enhanced heat and mass transfer efficiencies. Furthermore, the rapid and homogeneous mixing achieved in micro-fluidic devices promotes controlled nucleation and growth of crystalline particles [13].

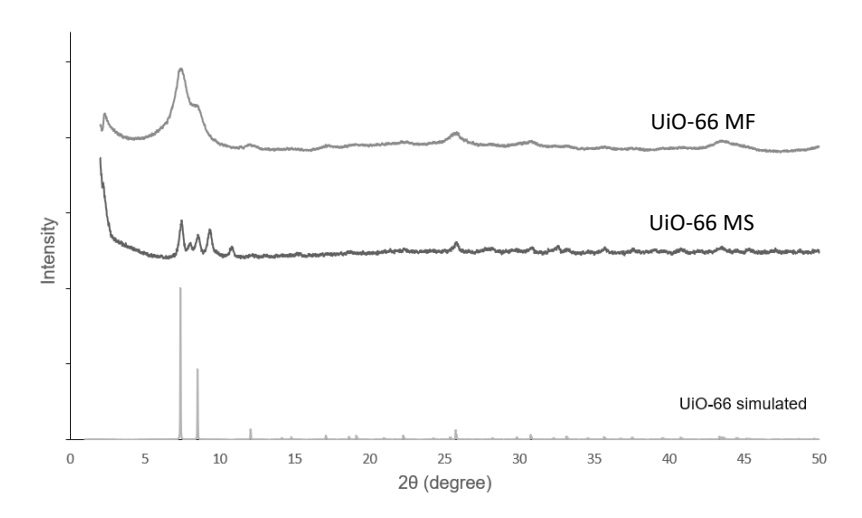


Fig. 1: XRD patterns of simulated and synthesized Zr-UiO-66 via macro-stationary (MS) and micro-fluidic (MF) routes.

Table 1: Comparison of crystal structures of UiO-66 particles synthesized via two different routes

Route	Crystallinity (%)	Crystallite size (nm)	Average particle size (nm)
Macro-stationary	62.5	22.7	20
Micro-fluidic	72.1	9.42	14

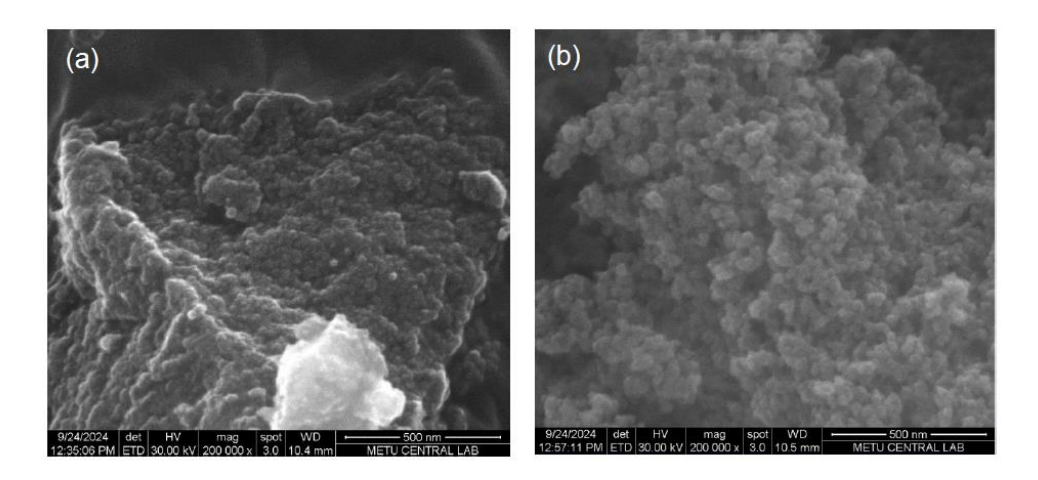


Fig 2: SEM images (at 200000x) of Zr-UiO-66 nanoparticles synthesized via (a) micro-fluidic and (b) macro-stationary routes.

# 3.2. Phosphate Adsorption Kinetics of Zr-UiO-66 Particles

Progressive uptake of phosphorus (P) by the adsorbent material Zr-UiO-66, indicated by a decrease in the concentration of aqueous P, during adsorption experiments conducted at 25, 50, 75, and 100 mg/L is presented in Figure 3. The rate of reduction in concentration is most pronounced during the first 20 minutes, after which the rate diminishes as the system approaches an equilibrium state. Higher initial concentrations resulted in higher residual phosphorus concentrations indication of limited phosphorus uptake by the adsorbent.

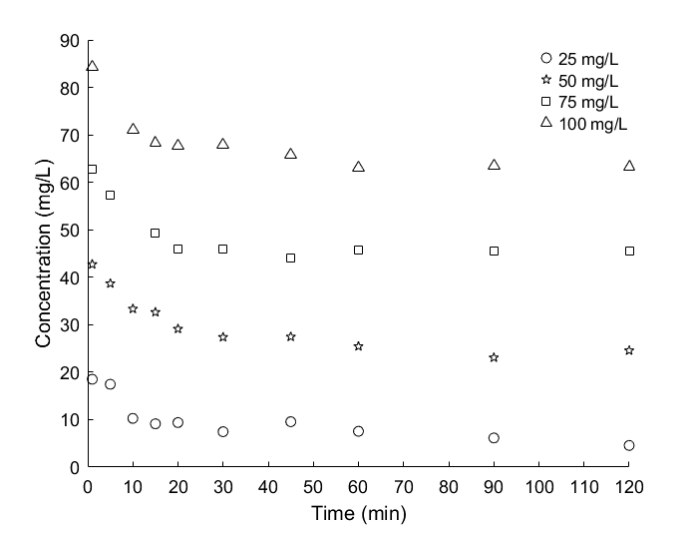


Fig 3: Concentration with time at initial P concentrations of 25, 50, 75, and 100 mg/L using macro-stationary synthesized Zr-UiO-66.

To quantitatively analyze the adsorption kinetics,  $q_t$  (mg/g) showing the amount of phosphorus adsorbed per unit mass of adsorbent at time t, was calculated for each experimental data point based on a mass balance given by  $q_t = (C_0 - C_t)V/m$ , where  $C_0$  is the initial P concentration (mg/L),  $C_t$  is the P concentration (mg/L) at the time of the data point, V is the volume of the solution (L), and m is the amount of adsorbent UiO-66 used (g). To elucidate the rate-controlling mechanisms, calculated results for  $q_t$  versus t were fitted to the pseudo-first-order kinetic rate equation given by:

$$\ln(q_e - q_t) = \ln q_e - \frac{k_1 t}{2.303} \tag{1}$$

and the pseudo-second-order kinetic rate equation given by:

$$\frac{t}{q_t} = \frac{1}{k_2 q_e^2} + \frac{t}{q_e} \tag{2}$$

where  $q_e$  (mg/g) is the amount of solute, i.e. phosphorus, adsorbed per unit mass of UiO-66 at equilibrium,  $k_l$  (min<sup>-1</sup>) is the pseudo-first-order rate constant and  $k_2$  (g/mg.min) is the pseudo-second-order rate constant. Fitting the adsorption data revealed that the pseudo-second-order kinetic model consistently yielded higher correlation coefficients (R²) compared to the pseudo-first-order model for all initial concentrations tested. The derived kinetic constants for both models are presented in Table 2. The observed adsorption kinetics, represented with a pseudo-second order fit in Figure 4, are consistent with the previously reported findings by Liu et al. [14] and Lin et al. [15].

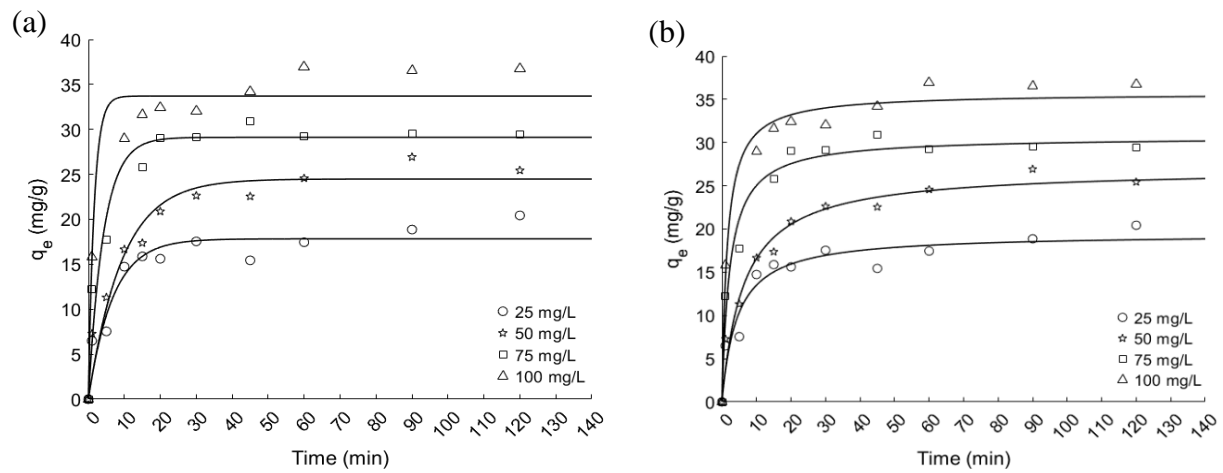


Fig 4: Phosphate adsorption data and kinetic models based on (a) pseudo-first-order and (b) pseudo-second-order rate equations.

Table 2: Kinetic constants of pseudo-first order and pseudo-second order rate equations for phosphate adsorption with UiO-66

	Pseudo-first order rate equation			Pseudo-second order rate equation		
$C_{\theta}(mg/L)$	$\mathbf{k_1}$ (min <sup>-1</sup> )	q <sub>e,est</sub>	$\mathbb{R}_{1}^{2}$	k <sub>2</sub> (g mg <sup>-1</sup> min <sup>-1</sup> )	<b>Q</b> e,est	$\mathbb{R}_2^2$
25	0.3400	17.8299	0.909	0.0117	19.4415	0.930
50	0.2457	24.4836	0.943	0.0059	26.9901	0.971
75	0.5456	29.1171	0.943	0.0145	30.6598	0.972
100	1.4325	33.7045	0.953	0.0186	35.7123	0.983

Langmuir and Freundlich isotherm models were fitted to the experimental data to evaluate the adsorption equilibrium. The Langmuir model assumes monolayer adsorption onto a surface characterized by a finite number of identical adsorptive sites. This model implies the existence of a maximum adsorption capacity,  $q_{max}$ , and the model is given by:

$$\frac{C_e}{q_e} = \frac{1}{K_L q_{max}} + \frac{C_e}{q_{max}}$$
where  $K_L$  represents the Langmuir adsorption constant in the equation. The resulting graph from the fitting is given in Figure

where  $K_L$  represents the Langmuir adsorption constant in the equation. The resulting graph from the fitting is given in Figure 5(a) with the corresponding constants given in Table 3. The  $R_L^2$  indicated a poor fit for this adsorption equilibrium. In contrast, the Freundlich isotherm assumes both monolayer and multiple layer adsorption, thereby accommodating the heterogeneous nature of the adsorbent surface. The Freundlich model is given by:

$$q_e = K_F C_e^{1/n} \tag{4}$$

where 1/n is the heterogeneity factor and  $K_F$  is the Freundlich adsorption constant. The constants and correlation coefficient,  $R_F^2$ , for the Freundlich adsorption curve shown in Figure 5(b) are presented in Table 3.

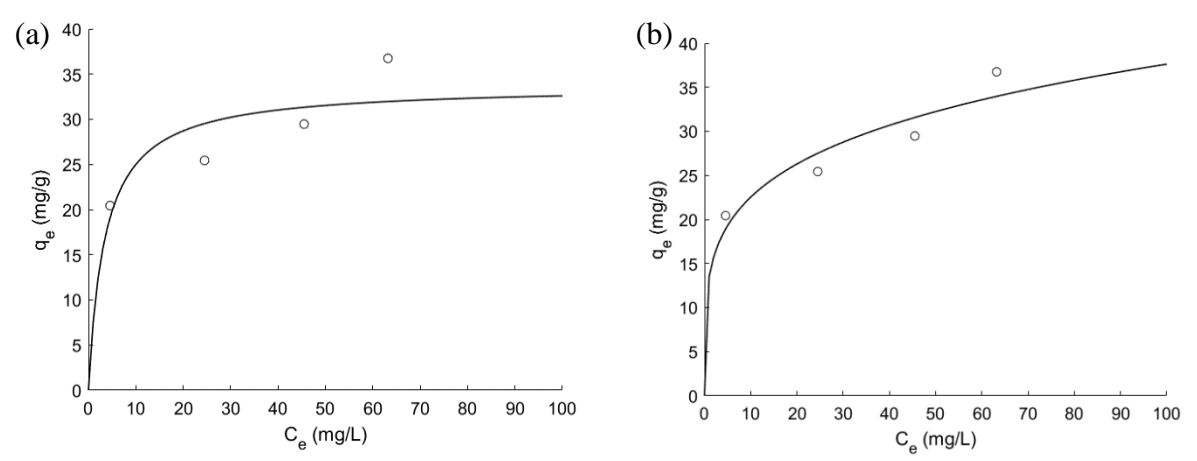


Fig 5: Experimental adsorption capacity data fitted to (a) Langmuir and (b) Freundlich isotherm models.

Table 3: Model constants of Langmuir and Freundlich adsorption isotherms

Langmuir		Freundlich			
$\mathbf{K}_{\mathbf{L}}$	q <sub>max</sub>	$\mathbf{R}\mathbf{L^2}$	$\mathbf{K}_{\mathbf{F}}$	n	$ m R_{F}^{2}$
0.29	33.74	0.69	13.49	4.49	0.86

To gain insight into the thermodynamics of the adsorption process, the change in free energy ( $\Delta G$ ) was calculated using:

$$\Delta G = -RT \ln(K) \tag{5}$$

Thermodynamic equilibrium constant (K) for the adsorption process was determined using the Freundlich constant, owing to the superior fit of the Freundlich isotherm to the experimental data. Calculations were performed at 298 K room temperature and utilizing the universal gas constant R as 8.314 J/mol.K. The  $\Delta G$  was calculated as -1.43 kJ/mol. This value is comparatively smaller than -4.112 kJ/mol reported by Liu et al. [14] at 298 K for phosphate adsorption on cerium-doped UiO-66. The negative value of  $\Delta G$  indicates the spontaneous nature of the adsorption process. The relatively small value of  $\Delta G$  suggests that physisorption is likely the predominant mechanism governing the interaction between UiO-66 and phosphate.

#### 3.3. Comparison of Phosphate Adsorption for Micro-fluidic and Macro-Stationary Synthesized UiO-66

A similar experimental protocol was applied to the micro-fluidic synthesized Zr-UiO-66 nanoparticles to facilitate a comparison with the macro-stationary synthesized material. However, the inherently lower product yield from the micro-fluidic synthesis necessitated a reduced number of experimental runs. Phosphorus concentration profiles over time are depicted in Figure 6(a), while Figure 6(b) presents the pseudo-second-order kinetic model fits for both synthesis methods. The corresponding kinetic parameters are summarized in Table 4. Comparative adsorption curves presented in Figure 6(b) showed that UiO-66 nanoparticles synthesized via the micro-fluidic route demonstrated slightly enhanced phosphate removal efficiency.

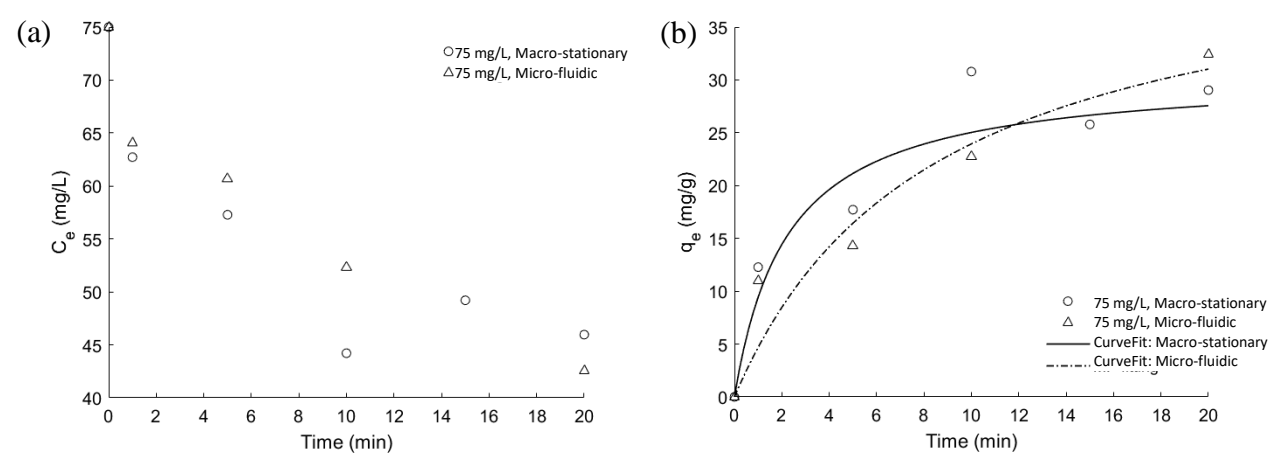


Fig 6: Comparison of phosphate (P) adsorption kinetics for macro-stationary and micro-fluidic synthesized Zr-UiO-66 at an initial concentration of 75 mg/L: (a) Temporal concentration profiles of P solutions, (b) Pseudo-second order kinetic model fits.

Table 4: Pseudo-second order kinetic constants for phosphate adsorption at 75 mg/L initial concentration on macro-stationary and micro-fluidic synthesized Zr-UiO-66

	Synthesis method	Pseudo-second order equation			
$C_0 (mg/L)$		k <sub>2</sub> (g mg <sup>-1</sup> min <sup>-1</sup> )	q <sub>e,est</sub>	$\mathbb{R}_2^2$	
75	Macro-stationary	0.0145	30.6598	0.972	
75	Micro-fluidic	0.0027	44.0669	0.921	

#### 4. Conclusion

Adsorption capacity, crystallinity, and particle size of Zr-UiO-66 crystals synthesized via conventional macrostationary and micro-fluidic methods were compared. The synthesis method significantly influenced the resulting material properties: The micro-fluidic approach yielded Zr-UiO-66 with smaller crystallites and higher overall crystallinity. These structural differences can impact the material's performance in applications, such as catalysis, adsorption, and gas storage. The adsorption process followed the pseudo-second order kinetics and fitted best with Freundlich isotherm, indicating heterogeneous binding sites. The calculated negative and relatively small change in Gibbs free energy ( $\Delta G$ ) confirmed a spontaneous, physisorption-dominated adsorption process. Comparative studies showed that micro-fluidic synthesized Zr-UiO-66 nanoparticles demonstrated slightly enhanced phosphate removal efficiency. Despite its advantages, the current micro-fluidic synthesis method suffers from limited yield, restricting comprehensive analysis. Future work should focus on improving micro-fluidic synthesis yields to enable more extensive experimental validation.

# **Acknowledgements**

This study is supported by The Scientific and Technological Research Institution of Turkiye (TUBITAK) through the 2224-A Grant Program for Participation in Scientific Meetings Abroad, 1001 Research Projects Funding Program project no:220M002, and BIDEB2209-A project no: 1919B012310536 and by Hacettepe University BAP project no: FHD-2024-20812. The authors would like to thank Dr. Ali Tuncel and Duygu Haciefendioglu of Department of Chemical Engineering at Hacettepe University for UV-Vis spectroscopy measurements.

#### References

- [1] S. R. Carpenter, "Eutrophication of aquatic ecosystems: Bistability and soil phosphorus," *Proceedings of the National Academy of Sciences*, vol. 102, no. 29, pp. 10002–10005, Jun. 2005. doi:10.1073/pnas.0503959102
- [2] L. E. de-Bashan and Y. Bashan, "Recent advances in removing phosphorus from wastewater and its future use as fertilizer (1997–2003)," *Water Research*, vol. 38, no. 19, pp. 4222–4246, Nov. 2004. doi:10.1016/j.watres.2004.07.014
- [3] A. N. Onar, N. Balkaya, and T. Akyüz, "Phosphate removal by adsorption," *Environmental Technology*, vol. 17, no. 2, pp. 207–213, Feb. 1996. doi:10.1080/09593331708616378
- [4] Y. Mei, X.-H. Zhu, L. Gao, H. Zhou, Y.-J. Xiang, and F. Liu, "Phosphorus adsorption/desorption kinetics of bioretention," *Thermal Science*, vol. 24, no. 4, pp. 2401–2410, 2020. doi:10.2298/tsci2004401m
- [5] Y. He, H. Lin, Y. Dong, and L. Wang, "Preferable adsorption of phosphate using lanthanum-incorporated porous zeolite: Characteristics and mechanism," *Applied Surface Science*, vol. 426, pp. 995–1004, Dec. 2017. doi:10.1016/j.apsusc.2017.07.272
- [6] M. Ramesh and C. Deepa, "Metal-organic frameworks and their composites," *Metal-Organic Frameworks for Chemical Reactions*, pp. 1–18, 2021. doi:10.1016/b978-0-12-822099-3.00001-0
- [7] A. Uzun and S. Keskin, "Site characteristics in metal organic frameworks for Gas Adsorption," *Progress in Surface Science*, vol. 89, no. 1, pp. 56–79, Feb. 2014. doi:10.1016/j.progsurf.2013.11.001
- [8] B. Chen and G. Qian, Metal-Organic Frameworks for Photonics Applications. Heidelberg, Berlin: Springer, 2016.
- [9] D. Boskovic and S. Loebbecke, "Synthesis of polymer particles and capsules employing micro-fluidic techniques," *nano Online*, Jan. 2016. doi:10.1515/nano.0034.00070
- [10] C. A. Serra and Z. Chang, "Micro-fluidic-assisted synthesis of polymer particles," *Chemical Engineering & Engineering & Technology*, vol. 31, no. 8, pp. 1099–1115, Jul. 2008. doi:10.1002/ceat.200800219
- [11] A. Vansteene, J.-P. Jasmin, S. Cavadias, C. Mariet, and G. Cote, "Towards chip prototyping: A model for droplet formation at both T and X-junctions in dripping regime," *Microfluidics and Nanofluidics*, vol. 22, no. 6, May 2018. doi:10.1007/s10404-018-2080-2
- [12] P. S. Chen, T. Y. Toribara, and Huber. Warner, "Microdetermination of phosphorus," *Analytical Chemistry*, vol. 28, no. 11, pp. 1756–1758, Nov. 1956. doi:10.1021/ac60119a033
- [13] Z. Liu, F. Fontana, A. Python, J. T. Hirvonen, and H. A. Santos, "Micro-fluidics for production of particles: Mechanism, methodology, and applications," *Small*, vol. 16, no. 9, Nov. 2019. doi:10.1002/smll.201904673
- [14] M. Liu, S. Li, N. Tang, Y. Wang, X. Yang, and S. Wang, "Highly efficient capture of phosphate from water via cerium-doped metal-organic frameworks," *Journal of Cleaner Production*, vol. 265, p. 121782, Aug. 2020. doi:10.1016/j.jclepro.2020.121782
- [15] K.-Y. A. Lin, S.-Y. Chen, and A. P. Jochems, "Zirconium-based metal organic frameworks: Highly selective adsorbents for removal of phosphate from water and urine," *Materials Chemistry and Physics*, vol. 160, pp. 168–176, Jun. 2015. doi:10.1016/j.matchemphys.2015.04.021